

High-efficiency MoRu–Be multilayer-coated gratings operating near normal incidence in the 11.1–12.0-nm wavelength range

John F. Seely, Claude Montcalm, Sherry Baker, and Saša Bajt

MoRu–Be multilayer coatings were applied to two diffraction gratings for the purpose of enhancing their normal-incidence efficiency in the 11.1–12.0-nm wavelength range. The grating substrates were replicas of a holographic master grating that had a blazed groove profile with 2400 grooves/mm and a 2-m radius of curvature. The relatively low average microroughness (0.8 nm) of the grating surfaces contributed to the relatively high groove efficiency of the grating substrates and the reflectance of the MoRu–Be multilayer coatings. The peak efficiency, measured with synchrotron radiation, was 10.4% in the second diffraction order at a wavelength of 11.37 nm.

OCIS codes: 050.1950, 310.6860, 340.7470.

1. Introduction

Multilayer interference coatings with high reflectance in the extreme-ultraviolet (EUV) wavelength region can dramatically enhance the normal-incidence efficiencies of diffraction gratings.^{1,2} The development of multilayer-coated gratings providing high efficiency and dispersion in the EUV and soft-x-ray regions is therefore important for high-resolution spectroscopic studies of laboratory, solar, and astrophysical radiation sources.³

Most previous research has used multilayers consisting of alternating layers of Mo and Si, the scattering (absorber) material and the transmissive (spacer) material, respectively.^{1,2} Mo–Si multilayers deposited onto flat superpolished substrates with very low microroughness (<0.1 nm) can have reflectances as high as 67.4% at wavelengths longer than the Si *L* absorption edge at 12.42 nm.⁴ The multilayer coating must be designed to have high reflectance at a wavelength for which the groove efficiency of the grating substrate is also high. In the case of a blazed grating substrate with flat facets, the optimal

efficiency occurs in the diffraction order that satisfies the blaze condition, where the incident radiation is specularly reflected from the grating facets into the on-blaze order.⁵

To achieve a high multilayer reflectance and a high grating groove efficiency, it is necessary that the microroughness of the grating substrate be much smaller than the wavelength of the incident radiation. On the basis of the characterization of various grating substrates using atomic-force microscopy and of the measured efficiencies of multilayer-coated gratings, it has been determined that grating substrates produced by a holographic process are typically superior to mechanically ruled gratings.⁶ The superior performance of multilayer-coated holographically produced gratings was attributed to the low microroughness and regular groove profile of the grating substrates. The holographic groove profiles of these gratings were shaped by ion-beam etching to produce a blazed (approximately triangular) groove profile or a laminar (rectangular) groove profile.^{1,2}

In this paper we report on the application of MoRu–Be multilayer interference reflection coatings to two replica gratings produced from a holographic, blazed master grating. A preliminary account of the efficiency performance of one of the gratings was given in Ref. 7. The use of Be as the transmissive spacer material permits the operation of the grating at wavelengths as short as the Be *K* absorption edge at 11.07 nm. In addition, the MoRu–Be multilayers have the beneficial property of smoothing the initial microroughness of the grating substrate. The effi-

J. F. Seely (john.seely@nrl.navy.mil) is with the Space Science Division, Naval Research Laboratory, Code 7674, Washington D.C. 20375. C. Montcalm, S. Baker, and S. Bajt are with the Department of Information Science and Technology, Lawrence Livermore National Laboratory, P.O. Box 808, L-395, Livermore, California 94551.

Received 6 October 2000; revised manuscript received 15 June 2001.

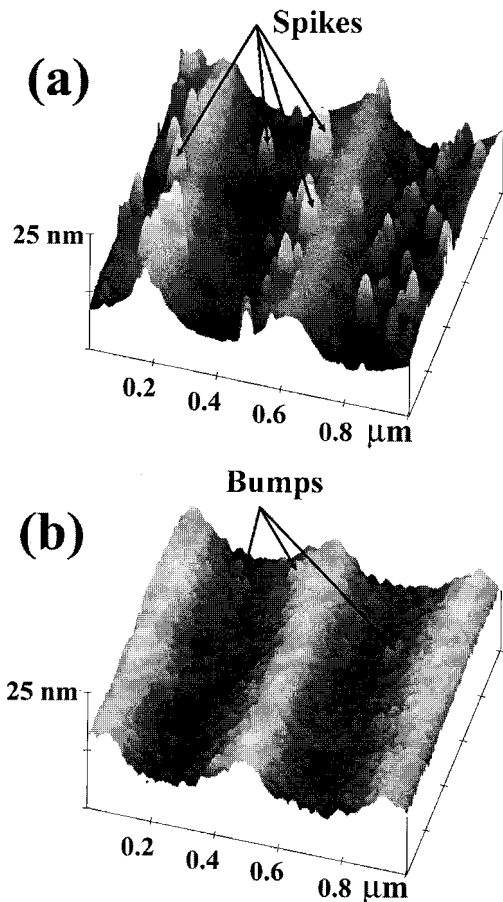


Fig. 1. AFM images of grating 2 (a) before and (b) after application of the MoRu–Be multilayer coating.

efficiencies of the multilayer-coated gratings, greatly enhanced by the high reflectance and smoothing properties of the MoRu–Be multilayer coatings, were measured with synchrotron radiation in the 10.5–13.0-nm wavelength range. A peak efficiency of 10.4% occurred in the second order at a wavelength of 11.37 nm. The efficiencies were also measured in the 25–50-nm wavelength range, where the reflectance occurred primarily from the topmost layers of the multilayer coatings. At the longer wavelengths, the first order had the highest efficiency. The measured efficiencies were compared with the efficiencies calculated from first principles by use of the modified integral method of Goray⁸ and Goray and Chernov.⁹ The shape of the blazed holographic groove profile was varied to achieve good overall agreement between the calculated and the measured efficiencies.

2. Holographic Blazed Gratings

The master grating, having 2400 grooves/mm and a 2-m concave radius of curvature, was produced by Spectrogon Inc., with a holographic technique. The blazed groove profile was shaped by ion-beam etching. The replica gratings were produced by Hyperfine Inc. Since the master grating was concave, a first-generation convex replica was produced, and concave replicas were subsequently produced from

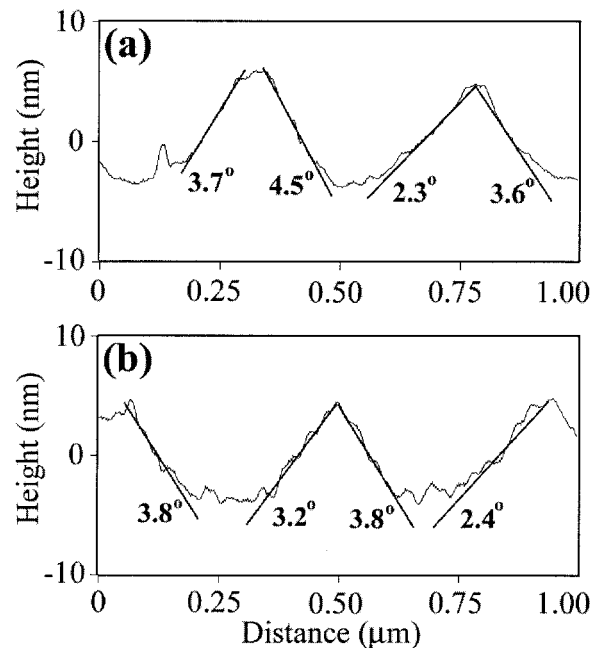


Fig. 2. Lineouts across the grooves of grating 2 (a) before and (b) after application of the MoRu–Be multilayer coating.

the convex replica. The surfaces of the replica gratings were oxidized aluminum. A thin overcoating of SiO₂ was applied to the final concave replicas for the purpose of reducing the microroughness of the oxidized aluminum surface.¹⁰

The surfaces of the concave replica gratings were characterized before and after the application of the MoRu–Be coatings by use of a Digital Instruments atomic-force microscope (AFM). The AFM was fitted with the following components: Dimension 5000 equipped with an acoustic hood, type G scanner, and a Nanoscope IIIA controller with phase extender box. The measurements were performed with a tapping mode that measures topography in air by tapping the surface with an oscillating probe tip. The probe tips were etched Si with a nominal tip radius of 5–10 nm. The roughness values (R_q) derived from the AFM measurements are the root-mean-square (rms) average of height deviations (z) taken from the mean data plane, expressed as

$$R_q = \left[\frac{(z_1^2 + z_2^2 + z_3^2 + \dots + z_N^2)}{N} \right]^{1/2}. \quad (1)$$

Shown in Fig. 1(a) is a $1 \mu\text{m} \times 1 \mu\text{m}$ image of the replica grating substrate before application of the MoRu–Be coating. The grating substrate had numerous spikes that were taller than the grooves. The typical heights were 10–12 nm, and base sizes were 60–70 nm. A lineout across the grooves in a region without spikes is shown in Fig. 2(a). This lineout illustrates the variation in the grooves and the facet angles. The average values of the facet angles of the left- and the right-facing facets are 3.0° and 4.1°, respectively. The deviations from the straight lines drawn on the facets in Fig. 2(a), mea-

sured near the centers of the facets, are in the 0.5–0.9-nm range. On the basis of the power spectral distribution that was derived from the AFM image shown in Fig. 1(a), the value of the microroughness in the $4\text{--}40\text{-}\mu\text{m}^{-1}$ spatial-frequency range was 1.35-nm rms. This range included the spikes that contributed significantly to the microroughness value.

3. MoRu–Be Multilayer Coatings

MoRu–Be multilayer coatings have recently been developed that have peak reflectances up to 69.3% at a wavelength of 11.4 nm.¹¹ The MoRu alloy material is believed to have a composition of Mo_4Ru_6 . The layers from this alloy remain amorphous in the multilayers, whereas the Be layers are polycrystalline. Such MoRu–Be multilayer coatings were applied to two replica grating substrates with a dc-magnetron sputtering system following a process described in Ref. 11. In this deposition system the substrates are held facedown by spinner assemblies mounted on a rotating platter and are swept over rectangular sputter sources with a controlled rotation velocity of the platter. The sputter chamber was typically cryopumped until the pressure was better than 1×10^{-7} Torr. Ultra-high-purity argon at a pressure of 0.9 mTorr was used to sputter the targets at source powers of 50–360 W. A perfect Mo_4Ru_6 –Be multilayer mirror would have a theoretical peak reflectance of 76% at a wavelength of 11.4 nm. However, because of imperfections, such as the roughness and diffusion of the interfaces and the surface oxidation, the highest achieved reflectance of an actual multilayer is somewhat lower.

Besides providing high reflectance, the MoRu–Be multilayer system offers several other beneficial properties.¹¹ The multilayer's stress, which is composition dependent, varies between -30 MPa and $+30$ MPa and can be designed to be nearly zero. Also, owing to the amorphous nature of the alloy layers, the coating smooths the high-frequency roughness of the substrate. For example, it has been shown that a 50-bilayer MoRu–Be coating, deposited on a substrate with 0.38-nm rms roughness with spatial frequencies between 4 and $40 \mu\text{m}^{-1}$, smoothed the substrate to 0.15-nm rms.¹¹

Multilayer coatings with 50 MoRu–Be bilayers were applied to the two grating substrates during separate deposition runs. Owing to a malfunction during the first deposition run, one grating was first coated with an incorrect multilayer with layers that were roughly ten times thicker than desired. This grating was subsequently overcoated with an additional 50 MoRu–Be bilayers with the proper layer thicknesses. Thus two multilayer gratings were produced, one with 50 MoRu–Be bilayers with the proper bilayer thickness (referred to as grating 1), and one with 100 MoRu–Be bilayers (grating 2) where the topmost 50 bilayers had the proper bilayer thickness. Calculations indicated that the multilayer interference reflection occurs primarily within the topmost 50 bilayers of each coating. Thus the

underlying 50 bilayers on grating 2 did not significantly affect the coating's reflectance.

The total thicknesses of the coatings on gratings 1 and 2 were 301.5 and >2000 nm, respectively. These coating thicknesses were much larger than the grating groove depth, which ranged from 6 to 8 nm. Thus the availability of two gratings with different coating thicknesses enabled the investigation of the effect of thick coatings on the grating efficiency. This is important because of previous evidence that a thick multilayer coating partially filled in the grooves of a laminar grating substrate.²

The comparison of the AFM images of grating 2 before and after application of the MoRu–Be coating provides striking evidence of the smoothing properties of the coating. As shown in Fig. 1(b), grating 2 after coating had numerous small bumps with heights that were much lower than the grooves. The bumps were also much smaller than the spikes seen before coating [Fig. 1(a)].

A lineout across the grooves of the coated grating 2 is shown in Fig. 2(b). The average angles of the left- and the right-facing facets are 2.8° and 3.8° , respectively. Within the groove-to-groove variation of the facet angles, the facet angles did not significantly change after coating. Thus the MoRu–Be coating tends to fill in around the tall (and high-spatial-frequency) spikes but not fill in the shallow (and low-frequency) grooves. The value of the microroughness derived from the AFM image shown in Fig. 1(b) in the $4\text{--}40\text{-}\mu\text{m}^{-1}$ spatial-frequency range, which includes the bumps, is 0.93-nm rms. This value is smaller than the 1.35-nm rms microroughness of the grating before coating. Since the efficiency of the multilayer-coated grating in the short-wavelength region is strongly dependent on the roughness, a multilayer coating that can smooth the grating surface is highly beneficial.

Prior to the deposition of the MoRu–Be multilayer coatings onto the two grating substrates, test coatings were deposited onto flat Si wafer substrates for the purpose of optimizing the bilayer thickness. The reflectances of the multilayer coatings, and the efficiencies of the multilayer gratings, were measured with the Naval Research Laboratory beamline X24C at the National Synchrotron Light Source at the Brookhaven National Laboratory. The synchrotron radiation was dispersed by a monochromator that had a resolving power of 600.^{12,13} Thin filters attenuated the radiation from the monochromator in the higher harmonics. The wavelength scale was established by the geometry of the monochromator and the absorption edges of the filters.

Figure 3(a) shows the reflectance of a typical test coating measured at an angle of incidence of 10° (squares) together with the best overall calculated fit to the measurements (dashed curve). This test multilayer coating had 20 bilayers instead of 50, a MoRu proportion of 0.42 relative to the total bilayer thickness, and a measured peak reflectance of 37.4% at a wavelength of 11.81 nm. The lower reflectance for this test multilayer, compared with the 69.3% reflec-

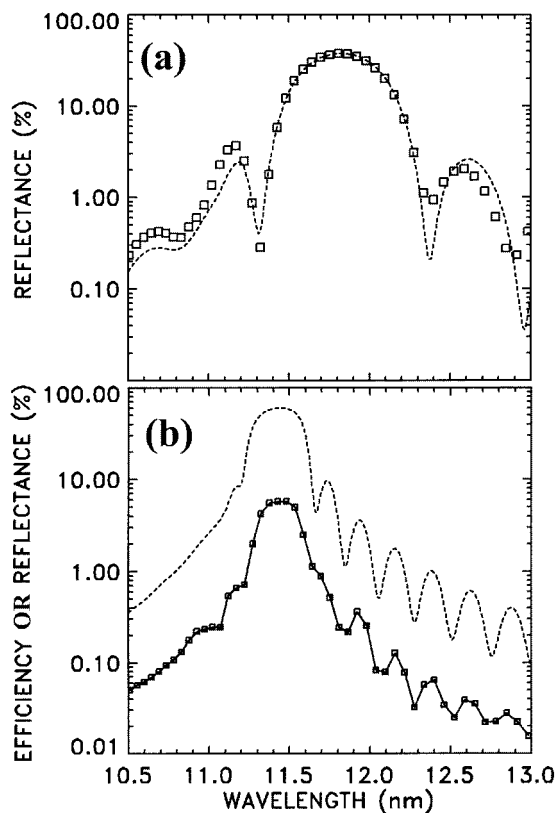


Fig. 3. (a) Measured (squares) and the calculated (dashed curve) reflectances of a test flat mirror with 20 MoRu-Be bilayers at an angle of incidence of 10° . (b) The zero-order efficiency of grating 1 measured at an angle of 13.9° (linked squares). Also shown is the predicted reflectance (dashed curve) of the multilayer coating with 50 MoRu-Be bilayers. The measured zero-order efficiency is a factor of 10 lower than the reflectance.

tance reported earlier¹¹ for coatings with 50 bilayers, resulted from the reduced number of bilayers (20) of the test multilayer.

The theoretical fit in Fig. 3(a) was calculated with the software IMD by Windt,¹⁴ assuming a 6.18-nm bilayer thickness and an interface roughness of 0.8 nm modeled by an error function profile. The optical constants were derived from the Center for X-Ray Optics scattering factors¹⁵ assuming a density of 11.4 g/cm^3 for the Mo_4Ru_6 layers and 1.85 g/cm^3 for the Be layers. It was also assumed that the topmost Be layer was partially oxidized, i.e., 2.9 nm of the top pure Be had reacted with oxygen and formed 5.0 nm of BeO. The calculated and the measured reflectances of the test coating are in good agreement.

4. Measured Grating Efficiency

Each multilayer grating was mounted in the reflectometer at the Naval Research Laboratory beamline X24C so that the dispersed radiation from the monochromator was incident on the center of the grating at an angle of 13.9° measured from the normal to the surface of the grating substrate. The 13.9° angle of incidence permitted the observation of a wide angular range without obscuration of the higher diffrac-

tion orders by the detector. The grating was oriented so that the groove facets with the larger facet angles faced the incident beam. The incident beam was approximately 1 mm in diameter. The incident radiation was approximately 80% polarized with the electric field vector in the plane of incidence. In this orientation the electric field vector was perpendicular to the grating grooves.

At fixed incident wavelengths the detector was scanned in angle about the grating and through the diffraction orders. Measurements were performed at a number of fixed wavelengths in the 10.5–13.0-nm range. After the angular position of the zero grating order was established, the detector was placed at the zero-order position and the wavelength was scanned. The zero-order efficiency of grating 1, measured at an angle of incidence of 13.9° , is shown in Fig. 3(b) (linked squares). The dashed curve in Fig. 3(b) shows the theoretical reflectance of the 50-bilayer MoRu-Be multilayer coating calculated with the same parameters used for the fit of the test coating shown in Fig. 3(a), except for the bilayer thickness, Λ , which was adjusted to 6.03 nm to better match the peak position. On the basis of this calculation, a peak reflectance of approximately 60% would have been obtained with this multilayer if deposited on a flat surface. In Fig. 3(b) the amplitude of the zero-order efficiency is ~ 10 times smaller than the reflectance, because of the groove efficiency of the grating substrate. The groove efficiency, defined as the ratio of the grating efficiency and the coating reflectance, is less than unity.

The grating pattern did not extend to the edge of the grating substrate, and it was possible to measure the multilayer reflectance on the flat region near the edge. The multilayer's bilayer thickness Λ , inferred from the comparison of the measured and the calculated reflectance profiles, was in agreement with the value 6.03 nm that was inferred from the measured zero-order efficiency.

The measured zero-order efficiencies of gratings 1 and 2 are compared in Fig. 4(a). The peak zero-order efficiencies are 6%. The peak efficiencies occur at wavelengths of 11.45 and 11.60 nm for gratings 1 and 2, respectively, and this indicates that the bilayer thicknesses of the multilayer coatings on the two gratings are slightly different. The calculated multilayer reflectance curves are shown in Fig. 4(b), where the bilayer thicknesses Λ are 6.03 and 6.11 nm for gratings 1 and 2, respectively.

The efficiencies in the various diffraction orders of grating 2, measured by means of scanning the detector in angle about the grating, are shown in Fig. 5 for an angle of incidence of 13.9° and an incident wavelength of 11.59 nm. The inside orders, with diffraction angles between the incident beam and the zero order, are indicated by positive-order numbers. The outside orders, with diffraction angles larger than the zero order, are indicated by negative-order numbers. The highest efficiency occurred in the -2 order. The 0.5° widths (at the half-peak efficiency levels) of the orders shown in Fig. 5 resulted from the 1-mm size of

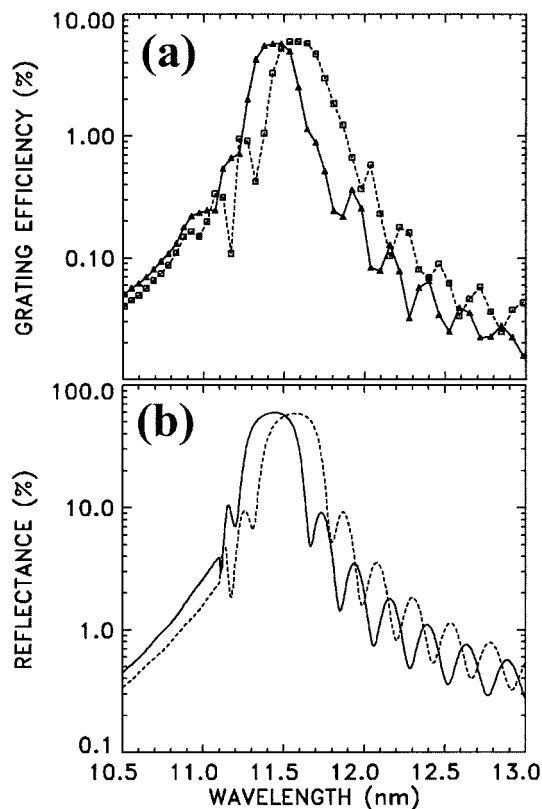


Fig. 4. (a) Solid and dashed curves are the measured zero-order efficiencies of multilayer gratings 1 and 2, respectively, at angles of incidence of 13.9° . (b) Solid and dashed curves are the calculated reflectances of the MoRu-Be multilayer coatings on grating 1 ($\Lambda = 6.03$ nm) and grating 2 ($\Lambda = 6.11$ nm), respectively. The angle of incidence is 13.9° , and the number of MoRu-Be bilayers is 50.

the incident radiation beam and the 1-mm slit over the detector.

As shown in Fig. 5, efficiencies as low as 0.02% could be accurately measured. This was made possible by the relatively high reflectance of the multi-

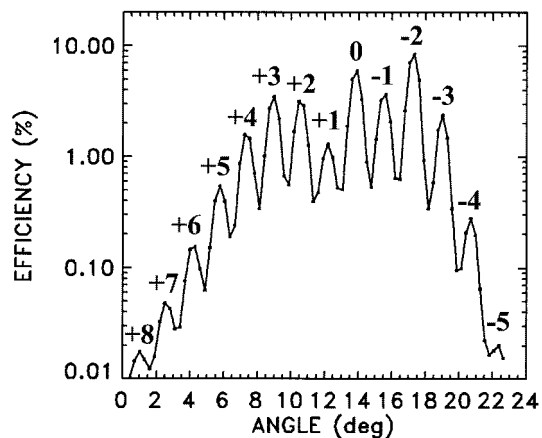


Fig. 5. Efficiency of multilayer grating 2 measured at an angle of incidence of 13.9° and for an incident wavelength of 11.59 nm. The inside orders (positive order numbers) and the outside orders (negative order numbers) are identified.

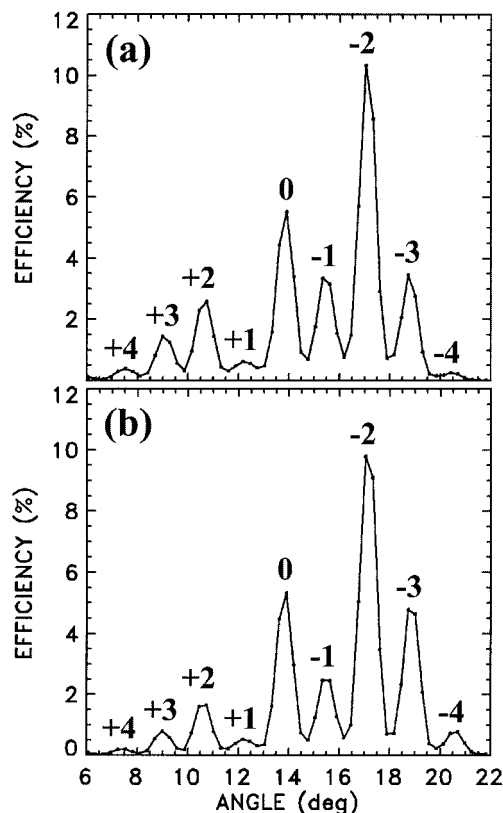


Fig. 6. Measured efficiencies of (a) grating 1 at a wavelength of 11.37 nm and (b) grating 2 at 11.48 nm. The angle of incidence was 13.9° .

layer and groove efficiency of the grating and by the high sensitivity and low background current (3 pA) of the Si photodiode detector used in these experiments (type AXUV-100G, provided by International Radiation Detectors Inc.). The efficiencies of grating 1 measured at an incident wavelength of 11.37 nm and grating 2 at 11.48 nm are shown in Figs. 6(a) and 6(b), respectively. The measured efficiencies of the two gratings are quite similar.

The measured peak efficiencies as functions of the incident wavelength are shown in Figs. 7(a) and 7(b) for gratings 1 and 2, respectively. The -2 order has the highest efficiency, peaking in the 11.4–11.5-nm wavelength region. The higher outside orders tend to have larger efficiencies at shorter wavelengths, and the inside orders have larger efficiencies at longer wavelengths. The envelopes of the grating efficiencies in the various orders are restricted in wavelength by the multilayer reflectance profiles shown in Fig. 4(b).

Figures 7(a) and 7(b) indicate that the peak efficiencies of grating 1 occurred at a slightly shorter wavelength compared with grating 2. This resulted from the smaller bilayer thickness on grating 1 as indicated by the measured zero-order efficiencies and the calculated multilayer reflectances shown in Fig. 4.

To a first approximation, neglecting index-of-refraction corrections, a multilayer interference coat-

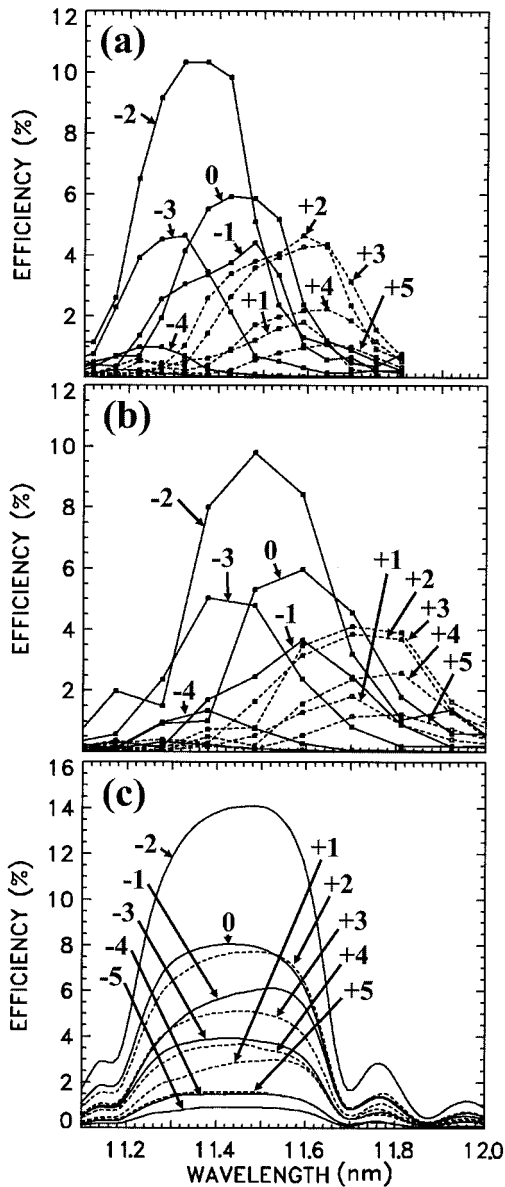


Fig. 7. Peak efficiencies measured at an angle of incidence of 13.9° for (a) grating 1 and (b) grating 2. (c) The calculated efficiencies at an angle of incidence of 13.9°.

ing has peak reflectance at a wavelength that satisfies the Bragg condition $\lambda = 2d \sin \theta$, where $2d$ is twice the bilayer thickness and θ is the grazing angle. The multilayer grating efficiencies were measured at three wavelengths (26.4, 35.4, and 49.6 nm) that are much larger than twice the bilayer thickness. Owing to the large attenuation coefficients of MoRu and Be at these longer wavelengths, the reflectance is primarily from the topmost few layers of the multilayer coating, and the interference effect is minimal since λ is much greater than $2d \sin \theta$. The grating efficiencies measured at a wavelength of 49.6 nm and at an angle of incidence of 13.9° are shown in Fig. 8(a) and 8(b) for grating 1 and grating 2, respectively. The peak efficiencies measured in the 25–50-nm wavelength range are shown in Figs. 9(a) and 9(b).

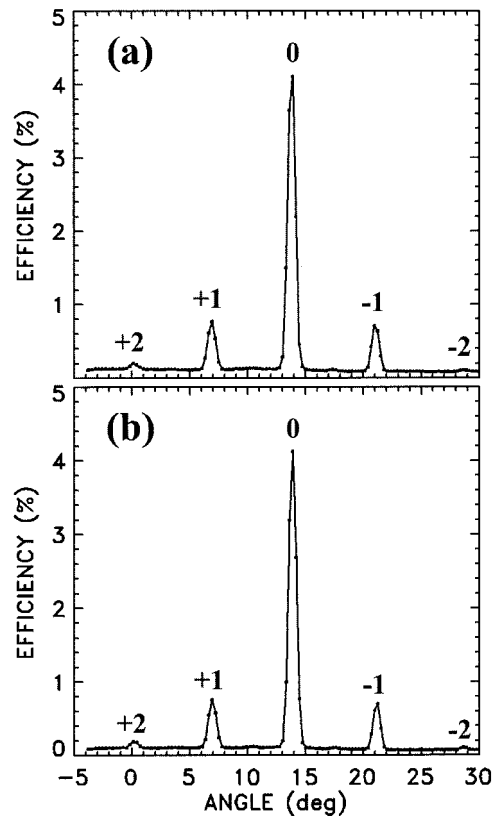


Fig. 8. Measured efficiencies of (a) grating 1 and (b) grating 2 at an angle of incidence of 13.9° and an incident wavelength of 49.6 nm.

The efficiencies are rather small because of the low normal-incidence reflectance in the absence of the multilayer interference enhancement. The efficiencies increase with wavelength primarily because the normal-incidence reflectance increases with wavelength in this spectral range. As shown in Section 5, the zero diffraction order has the highest groove efficiency in this wavelength region and results in high grating efficiency. Of the dispersed orders, the first orders have the highest efficiencies.

5. Calculated Grating Efficiency

The multilayer grating efficiency was calculated with the computational model (PCGRATE) developed by Goray⁸ and Goray and Chernov.⁹ The computational model implements the modified integral method to solve the boundary value problem of electromagnetic radiation incident on a multilayer grating. The calculation accounts for the groove profile of the grating substrate, the optical properties of the layers of the multilayer coating, and the two polarization components of the incident radiation. The computational model was previously used to analyze the efficiency of the uncoated replica grating substrate, and the calculated and the measured efficiencies were in good overall agreement.¹⁰

It was found that the calculated efficiencies of the MoRu–Be multilayer grating were sensitive to variations in the groove profile. Small changes in the

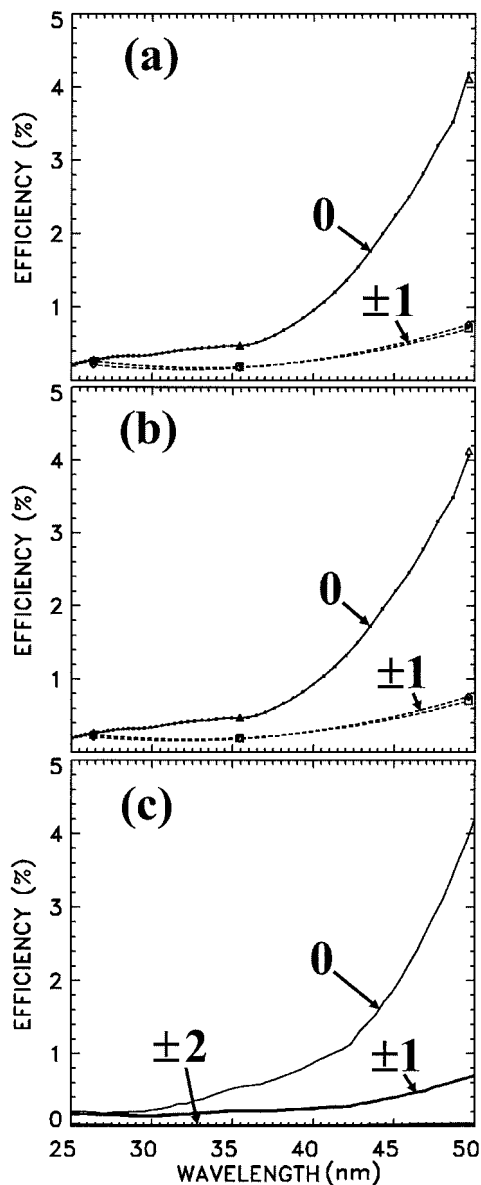


Fig. 9. Peak efficiencies measured at an angle of incidence of 13.9° of (a) grating 1 and (b) grating 2 as functions of wavelength. The large data points were derived from the detector scans at the three wavelengths 26.4, 35.4, and 49.6 nm. The dashed curves for the ± 1 orders are fits to the large data points. The solid curves with small data points are the zero-order efficiencies measured for wavelength scans over the 25.0–49.6-nm range. (c) The efficiencies calculated at an angle of incidence of 13.9° .

assumed groove shape, groove height, and facet angles resulted in significant changes in the calculated efficiencies. To facilitate the systematic study of the effect of the groove profile on the calculated efficiencies, an analytical function was chosen that was similar to the average groove profile of the grating as determined by AFM. The analytical function had parameters that allowed for variation of the groove shape, groove height, and facet angles. In this manner, the groove profile could be easily changed to obtain the best overall agreement with the measured efficiencies.

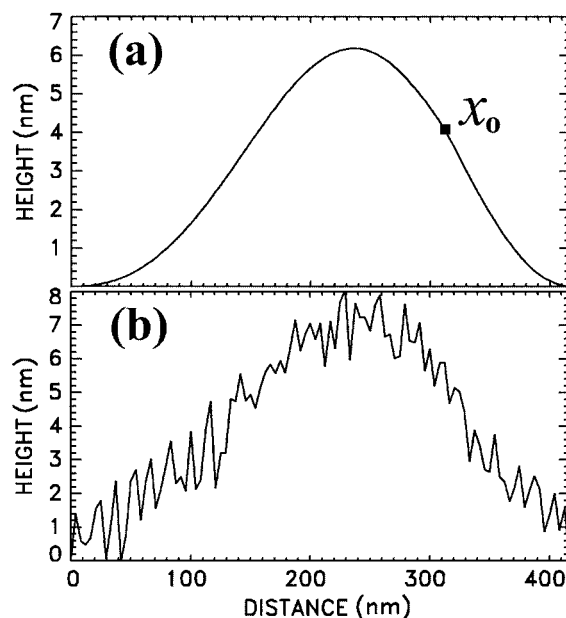


Fig. 10. (a) Analytical groove profile with height 6.2 nm. The left-hand side ($x \leq x_0$) of the profile is represented by the function $f(x)$ shown in Eq. (2) and the right-hand side ($x > x_0$) by the scaled $\sin(x)$ function. (b) The same groove profile but with a superimposed random microroughness having a standard deviation of 0.7 nm.

The analytical groove profile is defined as

$$f(x) = \int_0^x \sin t^n dt \quad (2)$$

for $0 \leq x \leq x_0$ and $\sin(x)$ for $x_0 < x \leq 1$, where x_0 is an inflection point of $f(x)$. The period and height of the $\sin(x)$ function were scaled so that the slope of the scaled $\sin(x)$ function was equal to the slope of $f(x)$ at x_0 . Thus $f(x)$ and the scaled $\sin(x)$ function connect smoothly at x_0 . If $n = 2$, then $f(x)$ is the Fresnel sine integral. The parameter n allows for the change in the shape of the groove profile. An additional adjustable parameter is the height of the groove profile. The groove profile for the case $n = 1.4$ and height 6.2 nm, which resulted in the best overall agreement between the calculated and the measured efficiencies, is shown in Fig. 10(a). The left-hand side of the profile ($x \leq x_0$) is represented by $f(x)$ and the right-hand side ($x > x_0$) by the scaled $\sin(x)$ function. The groove profile's horizontal extent has been set equal to the period (416.7 nm) of the grating pattern. The average angles of the flat portions of the groove profile, near the inflection points on the left- and the right-hand sides of the profile, are 2.6° and 3.5° . These angles are within the range of the facet angles derived from the AFM images of the two replica gratings. Shown in Fig. 10(b) is the same groove profile, consisting of 100 data points, and with a superimposed random microroughness with a standard deviation of 0.7 nm. The groove profile shown in Fig. 10(b) was used for the efficiency calculations.

A number of efficiency calculations were performed

by use of groove profiles with different shapes (different values of n) and different heights. The efficiencies changed significantly for changes in the shape parameter n of ± 0.1 and changes in groove height of ± 0.5 nm. In general, smaller values of n resulted in a straighter and flatter left facet and a narrower trough between the peaks of adjacent grooves. In this case, the narrow trough resulted in a lower zero-order efficiency and higher efficiencies in the dispersed orders. Larger values of n had the opposite effect. The left facet was more curved, and the trough was wider and flatter. The wider trough resulted in a higher zero-order efficiency and lower dispersed-order efficiencies.

An increase in the groove height resulted in larger facet angles, and the higher orders had increased efficiencies. Conversely, a lower groove height resulted in smaller facet angles and decreased efficiencies in the higher orders.

The calculated efficiencies, with a groove shape parameter of $n = 1.4$ and a groove height of 6.2 nm, are shown in Fig. 7(c) for the shorter-wavelength region enhanced by the multilayer reflectance and in Fig. 9(c) for the longer-wavelength region. In Fig. 7(c) the calculated peak efficiency (14%) in the -2 order is larger than measured (10.4% and 9.8%), and differences occur between the calculated and the measured efficiencies in the other dispersed orders.

In calculating the efficiencies in the longer-wavelength region (25–50 nm), it was found that using the optical constants derived from Henke *et al.*¹⁵ for the MoRu and Be layers resulted in poor agreement between the calculated and the measured efficiencies. Other calculations were performed with the optical constants from Refs. 16, 17, and 18 for Be, Mo, and Ru, respectively. The optical constants for Mo₄Ru₆ were derived from the optical constants of Mo and Ru assuming a density of 11.4 g/cm³. The topmost layer was assumed to be BeO with a density of 1.85 g/cm³. As seen in Fig. 9, the calculated and the measured efficiencies are in excellent agreement.

The normal-incidence efficiency of the uncoated replica grating, previously measured in the 14–22-nm wavelength range,¹⁰ was in good overall agreement with the efficiency calculated with the PCGRATE computer program. In general, considering the results of Ref. 10 and the present results, the efficiencies of blazed gratings that are calculated with PCGRATE are in good agreement at longer wavelengths (>14 nm), whereas significant differences occur at shorter wavelengths. The differences in the calculated and the measured efficiencies can provide guidance for future improvements in the computational model. For example, the differences at shorter wavelengths may indicate that the treatments of the groove and multilayer microroughness may need improvement.

6. Groove Efficiency

The groove efficiencies in the 5–20-nm wavelength range that were calculated with the optical constants derived from Henke *et al.*¹⁵ are shown in Fig. 11 for

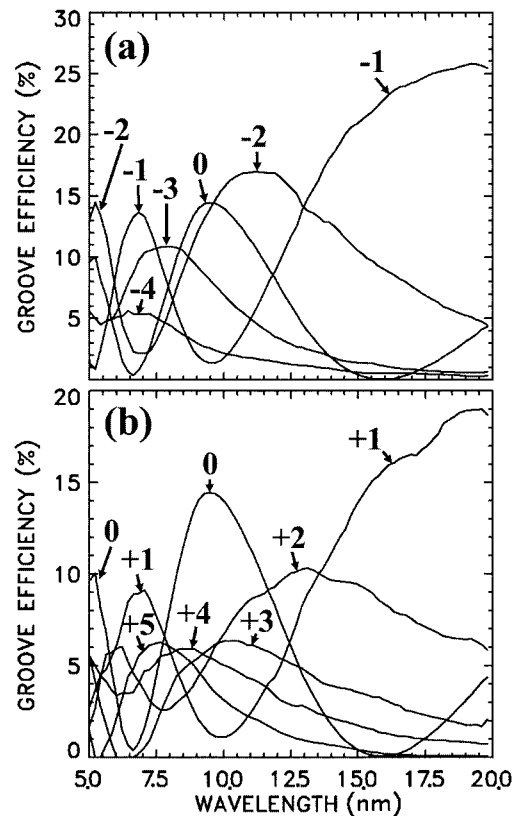


Fig. 11. Calculated groove efficiencies for (a) the outside orders and (b) the inside orders for an angle of incidence of 13.9°.

an angle of incidence of 13.9°. The outside-order groove efficiencies are shown in Fig. 11(a), and the inside-order groove efficiencies are shown in Fig. 11(b). The peak groove efficiencies are in the range 5–15% for wavelengths as short as 5 nm.

While differences between the calculated and the measured grating efficiencies occur in the 11.1–12.0-nm wavelength region (Fig. 7), the calculated groove efficiencies may be used as a guide for future experimental studies of the performance of multilayer-coated gratings at shorter wavelengths. These studies may be carried out by application of high-reflectance multilayer coatings to replica grating substrates of the same type used for the present study. When deposited on superpolished mirror substrates, multilayers with spacer layer materials such as C, B₄C, and Y have peak reflectances in the range 10–20% for wavelengths as short as 4.5 nm.¹⁹ However, the reflectances would be somewhat lower when deposited on a grating substrate with 0.8-nm microroughness. Since the grating efficiency is approximately equal to the product of the multilayer reflectance and the groove efficiency, peak grating efficiencies near 1–2% are expected. By comparison, the efficiency of the gold-coated grating on the Skylab space station, which recorded numerous well-exposed solar spectra, had a normal-incidence efficiency of 0.05–2% in the 17–35-nm wavelength range.^{6,20,21}

The calculated groove efficiencies shown in Fig. 11 have interesting oscillatory behaviors at wavelengths

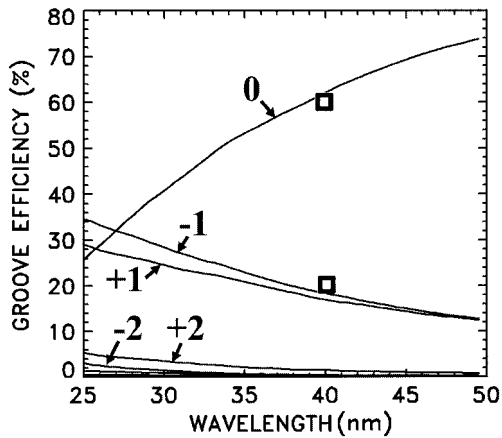


Fig. 12. Curves are the calculated groove efficiencies. The two data points at a wavelength of 40 nm are the measured groove efficiencies in the zero order and the ± 1 orders.

below 10 nm. The study of the grating performance with high-reflectance multilayer coatings will result in the experimental determination of the groove efficiency, which can be compared with the calculated groove efficiency. This information will be important for the improvement of the computational model for the groove efficiency in the short-wavelength region.

The relatively large calculated groove efficiencies in the higher inside orders shown in Fig. 11(b) are interesting. For example, the groove efficiency in the +5-order peaks at a wavelength of 7.5 nm. This suggests that both large angular dispersion and relatively large efficiency may be achievable in the 5–10-nm wavelength range. Large angular dispersion generally results in higher spectral resolution and higher spectral line to background detector signal levels, which are necessary for the implementation of spectroscopic diagnostic techniques.^{3,21}

The calculated groove efficiencies in the longer-wavelength region of 25–50 nm are shown in Fig. 12. The two data points at a wavelength of 40 nm are the groove efficiencies in the zero order and in the ± 1 orders that were inferred from the measurements in the following manner. The reflectance of the flat region near the edge of the grating was measured to be 1.5% at a wavelength of 40 nm and an angle of incidence of 16°. This value was in excellent agreement with the reflectance value (1.6%) that was calculated assuming a microroughness of 1.3 nm as inferred from the measured and the calculated reflectances at shorter wavelengths near the edge of the grating. The groove efficiency inferred from the measurements at a wavelength of 40 nm is the ratio of the measured efficiency, as shown in Figs. 9 (a) and 9(b), and the measured reflectance. The groove efficiencies inferred from the measurements are in good agreement with the calculated values as shown in Fig. 12.

At the upper end of the 25–50-nm wavelength range, the highest groove efficiency occurs in the zero order, and the groove efficiencies in the dispersed

orders are much smaller. The groove efficiency in the zero order increases with wavelength, and the dispersed orders decrease. The trends in groove efficiency at longer wavelengths are consistent with the small facet angles of the groove profile, the rounded shape of the groove profile, and the wide troughs between the grooves. These features of the groove profile tend to result in a high zero-order efficiency at longer wavelengths.

7. Summary

The normal-incidence efficiencies of two replicas of a holographic, blazed grating were dramatically enhanced by the application of MoRu–Be multilayer coatings. Although one grating had 50 MoRu–Be bilayers and the other grating had 100 bilayers and a much larger overall coating thickness, the multilayer reflectances and the efficiencies of the two gratings were practically the same. This indicated that the thicker coating did not degrade the grating performance, for example, by partially filling in the grating grooves.

The peak efficiency in the -2 order was 10.4% at a wavelength of 11.37 nm. To our knowledge, this is the first experimental demonstration of a normal-incidence multilayer grating at a wavelength below the Si *L* absorption edge at 12.42 nm. Modeling indicated that the small blaze angle (approximately 3°) and the low microroughness (0.8 nm) of the replica grating substrate may permit normal-incidence operation at wavelengths as short as 5 nm when an appropriate multilayer spacer material such as C, B₄C, or Y is used. For example, we are currently developing Mo–Y multilayer coatings for that purpose, which can provide 20–45% reflectances in the 8–12-nm wavelength region.²² In addition, the relatively large efficiencies expected in the higher inside orders may result in large angular dispersion and high spectral resolution.

The development of normal-incidence multilayer gratings that have high efficiencies in the soft-x-ray wavelength region will facilitate the implementation of high-resolution spectroscopic diagnostic techniques to determine the properties of hot laboratory, solar, and astrophysical plasmas.^{3,21} For example, a number of intense spectral lines are emitted from active stars in the 8–12-nm wavelength region, such as the Fe XVIII line at $\lambda = 9.4$ nm emitted by Capella.²³

This research was supported by NASA project W-19513. The research at Lawrence Livermore National Laboratory was performed under the auspices of the U.S. Department of Energy by the University of California Lawrence Livermore National Laboratory under contract W-7405-ENG-48. Part of the research was performed at the National Synchrotron Light Source, which is supported by the U.S. Department of Energy. The authors thank F. R. Grabner, R. D. Behymer, and M. Mao for their assistance in the setup of the system used for the deposition of the multilayer coatings.

References

1. J. F. Seely, R. G. Cruddace, M. P. Kowalski, W. R. Hunter, T. W. Barbee, J. C. Rife, R. Ely, and K. G. Stilt, "Polarization and efficiency of a concave multilayer grating in the 135–250-Å region and in normal-incidence and Seya–Maniœ mounts," *Appl. Opt.* **34**, 7347–7354 (1995).
2. J. F. Seely, M. P. Kowalski, R. G. Cruddace, K. F. Heidemann, U. Heinzmann, U. Kleineberg, K. Osterried, D. Menke, J. C. Rife, and W. R. Hunter, "Multilayer-coated laminar grating with 16% normal-incidence efficiency in the 150-Å wavelength region," *Appl. Opt.* **36**, 8206–8213 (1997).
3. U. Feldman, P. Mandelbaum, J. F. Seely, G. A. Doschek, and H. Gursky, "The potential for plasma diagnostics from stellar extreme-ultraviolet observations," *Astrophys. J. Suppl.* **81**, 387–408 (1992).
4. P. B. Mirkarimi, S. Bajt, and M. A. Wall, "Mo/Si and Mo/Be multilayer thin films on Zerodur substrates for extreme-ultraviolet lithography," *Appl. Opt.* **39**, 1617–1625 (2000).
5. J. F. Seely, M. P. Kowalski, W. R. Hunter, J. C. Rife, T. W. Barbee, G. E. Holland, C. N. Boyer, and C. M. Brown, "On-blaze operation of a Mo/Si multilayer-coated concave diffraction grating in the 136–142-Å wavelength region and near normal incidence," *Appl. Opt.* **32**, 4890–4897 (1993).
6. J. F. Seely, M. P. Kowalski, W. R. Hunter, T. W. Barbee, R. G. Cruddace, and J. C. Rife, "Normal-incidence efficiencies in the 115–340-Å wavelength region of replicas of the Skylab 3600 line/mm grating with multilayer and gold coatings," *Appl. Opt.* **34**, 6453–6458 (1995).
7. C. Montcalm, S. Bajt, and J. F. Seely, "MoRu–Be multilayer-coated grating with 10.4% normal-incidence efficiency near the 11.4-nm wavelength," *Opt. Lett.* **26**, 125–127 (2001).
8. L. I. Goray, "Numerical analysis for relief gratings working in the soft x-ray and XUV region by the integral equation method," in *X-Ray and UV Detectors*, R. B. Hoover and M. W. Tate, eds., *Proc. SPIE* **2278**, 168–172 (1994).
9. L. I. Goray and B. C. Chernov, "Comparison of rigorous methods for x-ray and XUV grating diffraction analysis," in *X-Ray and Extreme Ultraviolet Optics*, R. B. Hoover and A. B. C. Walker, eds., *Proc. SPIE* **2515**, 240–245 (1995).
10. J. F. Seely, L. I. Goray, W. R. Hunter, and J. C. Rife, "Thin-film interference effects on the efficiency of a normal-incidence grating in the 100–350-Å wavelength region," *Appl. Opt.* **38**, 1251–1258 (1999).
11. S. Bajt, "Molybdenum-ruthenium/beryllium multilayer coatings," *J. Vac. Sci. Technol. A* **18**, 557–559 (2000).
12. J. C. Rife, H. R. Sadeghi, and W. R. Hunter, "Upgrades and recent performance of the grating/crystal monochromator," *Rev. Sci. Instrum.* **60**, 2064–2067 (1989).
13. W. R. Hunter and J. C. Rife, "An ultrahigh vacuum reflectometer/goniometer for use with synchrotron radiation," *Nucl. Instrum. Methods A* **246**, 465–468 (1986).
14. D. L. Windt, "IMD: software for modeling the optical properties of multilayer films," *Comput. Phys.* **12**, 360–370 (1998). A copy of the software can be downloaded at <http://cletus.phys.columbia.edu/~windt/imd/>.
15. B. L. Henke, E. M. Gullikson, and J. C. Davis, "X-ray interactions: photoabsorption, scattering, transmission, and reflection at E=50–30,000 eV, Z=1–92," *At. Data Nucl. Data Tables* **54**, 181–342 (1993). Updated optical constants were obtained at http://www-cxro.lbl.gov/optical_constants/.
16. E. T. Arakawa, T. A. Callcott, and Y. C. Chang, "Beryllium (Be)," in *Handbook of Optical Constants of Solids II*, E. D. Palik, ed. (Academic, New York, 1991), pp. 421–433.
17. D. W. Lynch and W. R. Hunter, "Molybdenum (Mo)," in *Handbook of Optical Constants of Solids*, E. D. Palik, ed. (Academic, New York, 1985), pp. 303–313.
18. D. W. Lynch and W. R. Hunter, "Ruthenium (Ru)," in *Handbook of Optical Constants of Solids III*, E. D. Palik, ed. (Academic, New York, 1998), pp. 253–261.
19. A tabulation of measured normal incidence reflectances can be found at the Center for X-Ray Optics Internet site, <http://www-cxro.lbl.gov/multilayer/survey.html>.
20. R. Tousey, J.-D. Bartoe, G. E. Brueckner, and J. D. Purcell, "Extreme ultraviolet spectroheliograph ATM experiment SO82A," *Appl. Opt.* **16**, 870–878 (1977).
21. U. Feldman, J. D. Purcell, and B. Dohne, *An Atlas of Extreme Ultraviolet Spectroheliograms from 170 to 625 Å* (E. O. Hulburt Center for Space Research, Naval Research Laboratory, Washington, D.C., 1987).
22. C. Montcalm, B. T. Sullivan, M. Ranger, and H. Pépin, "Ultra-high vacuum deposition-reflectometer system for the *in situ* investigation of Y/Mo extreme-ultraviolet multilayer mirrors," *J. Vac. Sci. Technol. A* **15**, 3069–3081 (1997).
23. A. K. Dupree, N. S. Brickhouse, and G. J. Hanson, in *Astrophysics in the EUV*, International Astronomical Union Colloquium **152**, S. Bowyer and R. Malina, eds. (Kluwer, Dordrecht, The Netherlands, 1996), p. 141.